International Conference on Space Optics—ICSO 2014

La Caleta, Tenerife, Canary Islands

7–10 October 2014

The challenges for large light-weight diffractive lenses for space telescopes

S. Roose

Y. Stockman

D. Derauw

L. Datashvlli

et al.

THE CHALLENGES FOR LARGE LIGHT-WEIGHT DIFFRACTIVE LENSES FOR SPACE TELESCOPES.

S. Roose[1], Y. Stockman[1], D. Derauw[1], L. Datashvlli[2], H. Baier[2]

[1] Centre Spatial de Liège, Université de Liège, Avenue du Pré-Aily, B-4031 Angleur-Liège, Belgium.
[2] Lehrstuhl für Leichtbau, Technische Universität München, Boltzmannstraße 15, D-85747 Garching b. München, Germany)

I. INTRODUCTION

Large light-weight telescopes in space are considered key elements enabling future earth observation and space science. The first large space telescope, "Hubble", uses a monolithic aspheric primary mirror of 2.4 m diameter. The Hubble Space Telescope primary mirror has an area density of about 180 kg/m^2. This monolithic approach cannot be used for much larger telescopes due to mass and volume limitations imposed by today's launch capabilities. Thus the current generation space telescope, the James Webb Space Telescope now under development, makes use of a segmented aspheric primary mirror of 6.5 m diameter. The area density will be below 20 kg/m^2.

Continued demand for new science and observation from space will drive the need for even larger telescope apertures. This requires completely new concepts of deployable space telescopes with primary mirror aerial densities below 3 kg/m^2. Immediate candidates for such a low aerial density primary mirrors are Gossamer Structures. These consist of membranes or thin shells which can be easily stowed inside the launcher shroud and which will deploy once in orbit by inflation or by releasing a pre-stress. The required surface shape accuracies are very strict. For visible wavelengths, one requires sub-micrometric surface shape accuracies (10 nm -100 nm). These shape requirements can be relaxed to the order of a few μm, considering that the telescope has an active wavefront correction on board with this correction stroke (several micrometers).

An alternative to such strict shape requirements can pass by diffractive flat apertures which appear to have much more relaxed surface requirements.

Recent years numerous papers appeared in this field [1][2][3][4][5][6][7][8]. Some of them announcing dramatic revolution in the construction of space telescopes with a new revolutionary device: a photon sieve. This device is a diffractive lens, or in "optical jargon" a synthetic on-axis absorption hologram. Holographic or diffractive optical elements are nowadays common (requiring special manufacturing techniques) optical devices at scales of 0.1 m. Manufacturing and using them at 10 m scales is a huge step.

The European Space Agency (ESA) has recently funded a small ground-demonstrator project. We explored several aspects of the manufacturing of a space telescope with a diffractive lens. Most the challenges lie on the mechanical side, especially in modelling the thermo-elastic behaviour of this device under different thermal loads. A small scale photonsieve in aluminized Kapton. The results of this photonsieve are presented in this article too.

II. OPTICAL DESIGN ASPECTS

If one aims a 10 m diameter parabolic reflector with diffraction limited quality (@500 nm): this means that we want to have a surface shape error of typically less than 50 nm. This figure is independent of the size, the focal length and is a polishing challenge for the mirror manufacturer. This is the starting point of many authors to put forward large lightweight diffractive optics as an alternative for reflective optics, with the statement that it is cheaper.

While for reflective optics it is the gradient of the surface shape (the surface slope) which provides the re-orientation of the light rays, in diffractive optics it is the spatial frequencies (the local grating) that play a role in the light deflection. Indeed if one the example of a Fresnel Zone Plate, Small features act as a local grating, and light at the edges is more deflected than in the center.

This is mathematical representation of the transmission function of this element (Fig.1) can be done in terms of Fourier Series [9]. There is one Fourier component m=-1, which is called the first diffraction order, which reshapes the light as it was a lens with throughput. The relative irradiance of this component is $1/\pi$ or in terms of energy $1/\pi^2 = 10.1\%$. This is not an advantage with respect to a reflective telescope that focuses 100% of the light. We would need 9 times more area (increase the diameter by a factor 3) to collect the same amount of light. Diffractive optics experts will tell that one can move to a binary Fresnel lens type, which is fully transparent. The first diffraction order m=-1 has $4/\pi^2 = 40.5\%$ energy of the incoming wave.
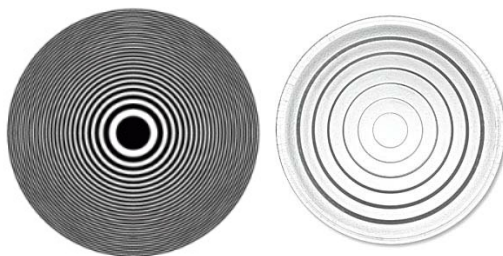
Fig.1. Fresnel Zone plate and binary Fresnel lens.

The phase function of this element is truly binary with local phase jumps of π, which can be realised by local optical path differences of π. For a Glass substrate (n=1.5), and wavelengths of 500 nm, the steps are 500 nm. Higher efficiency can be obtained with intermediate phase steps. The surface relief manufacturing accuracy (out of plane) is clearly, sub-micrometric with increasing demands in efficiency in the first diffraction order: We notice also that when the operational wavelength is not the design wavelength, the phase jump scales with $(1/\lambda)$. In the worst case the jump is $2.\pi$, the efficiency drops to zero.

A pure transparent transmission lens needs a surface relief structure on a transparent substrate. Absorptive diffractive optics (Fig.2) relies on the perforation of opaque substrates. No isolated substrate structures can be envisaged such as in Fresnel lens. Material continuity need to be guaranteed as shown in Fig.2.
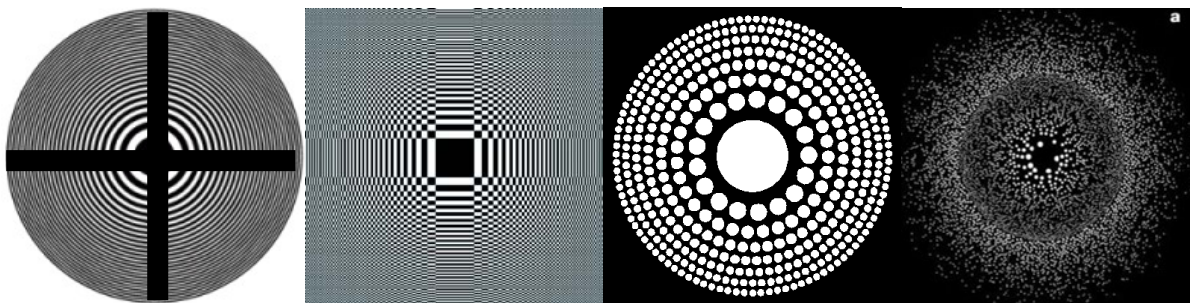
Fig.2. Different Fresnel lens types with substrate continuity. (a) Fresnel zone plate (FZP), (b) Crossed cylindrical lens FZP, (c) Photonsieve, (d) Photonsieve with anti-holes.

The center of the apertures in Fig.2 are all centered on the iso-phase modulo 2π lines, and will provided constructive interference and a diffraction limited image at distance "f", the focal length. The diffraction limited pattern however, especially its symmetry, will depend on the aperture size and distribution. Anyhow, because we increase the obscuration of the aperture, one will never reach the diffraction efficiency of 10.1%.

The transmission function equation tells also that the spatial distribution of the rings, corresponding to the π phase jumps, depends on the product "$f.\lambda_0$". The spatial frequency is dependent on a design wavelength. If the diffractive element is illuminated with the design wavelength, the angular light redistribution as predicted at that wavelength. For larger or smaller wavelengths the angular redistribution is respectively larger or smaller, as for diffraction gratings.

As for a diffraction grating it is a thin and flat element. While for reflective optics (non-flat), it is the shape and its manufacturing accuracy that affect the functional quality, here it is the in-plane positioning accuracy that plays a role. In the case a diffractive element with lens function the lower-bound is set lowest F-number:

$$\Delta x <<< \lambda_0.\text{F-number}$$
(For diffraction limited performances we need that local phase errors remain smaller than $\pi/4$)

These in-plane tolerances are of the orders of 10μm (@500 nm), for F–numbers larger than 20. The in-plane tolerances are relaxed for larger wavelength and larger F-numbers.

Current lithographic techniques allow reaching sub micrometric pattern on 200 mm diameters wafers. But what about a 10 m aperture? At larger scale thermo-elastic effects start to be important. A CTE of 10 ppm/K, and a difference of 1K in temperature will already give 200μm stretching. Temperature control of the substrate and local overheating might be a problem.

Homogenous temperature changes are not a real problem during the usage of the lens, it appears a scaling of focal length. But this is a dramatic constraint on the manufacturing facility because the dimensions need to remain stable during the duration of the lens manufacturing. In flight temperature gradients can also be a problem, because that would means that the focal length is not constant in the full aperture of the lens.

Diffractive optics is chromatic optics. The optical function scales with the wavelength. In the case of a lens function, the focal length shift is given by and for a fixed detector position, we have diffraction limited imaging for a narrow bandwidth (This is typically 0.001 nm for λ=500 nm, lens D= 10 m, f=200m).

It is widely recognized that this chromatism can be compensated with an achromatic lens that will image the diffractive element on a de-magnified one [10]. This is proposed as the solution to counterbalance chromatism. Several achromatic design configurations are propose by Meinel & Meinel' [11][12]. (Reflective an refractive solutions) at design level, but they always require a perfect imaging and high centring accuracy to image one diffractive element on the other one. If one aims 100 nm bandwidth, one shall have an achromatic corrector of corrector De=1 m for a diffractive lens of 10 m. A 1 m achromatic refractive corrector is not a small lightweight lens it can easily reach 500 kg. Achromatic can be corrected, but it increases the design complexity and number of optical components, and it has some effect on the mass budget, which can not be considered as a marginal add-on the system.

Given the large focal lengths , more than 100 m we shall envisage the use of two Formation Flying Spacecraft [1],[7] (lens satellite, detector satellite) ,which will have to be co-aligned and stabilized in space with 0.1 mm accuracy (λ0=500 nm, D= 10 m, f=200m).

These examples illustrate that most of the drawbacks of diffractive lenses can be bypassed, but theses solutions have unfortunately a price in terms of system complexity. Our conclusion would be that it is worthwhile to pursue the research in this field for applications where there is no alternative as reflective or refractive telescope.

III. MECHANICAL DESIGN ASPECTS

A. Materials

A first challenge from the mechanical side is to find adequate materials, which:

- Are machinable, this means that accept a transmission (black and white) pattern or a phase relief pattern.
- Are stowable and deployable
- Large operational temperature range
- Optically transparent or opaque

A brief survey allowed us to focus our attention on polyimides. Indeed, they are a class of high temperature-resistant polymers. These materials have high UV and gamma radiation resistance; excellent abrasion, wear, and chemical resistance; and high tensile strength with low creep. Their operating temperatures from cryogenic up to 400°C. They are transparent for visible wavelengths. Some polyimides can be designed with a near zero CTE (<1ppm/K) [15][17].

B. Deployment mechanisms

The lenses will be supported in space by their deployment mechanisms. In our study we investigated the use of pantograph system such as proposed on the flight tested Georgian mesh reflector [16]. The control of stretching of the membrane can be done with actuators mounted on a stiff (after deployment) outer-ring, which pretensions the membrane.
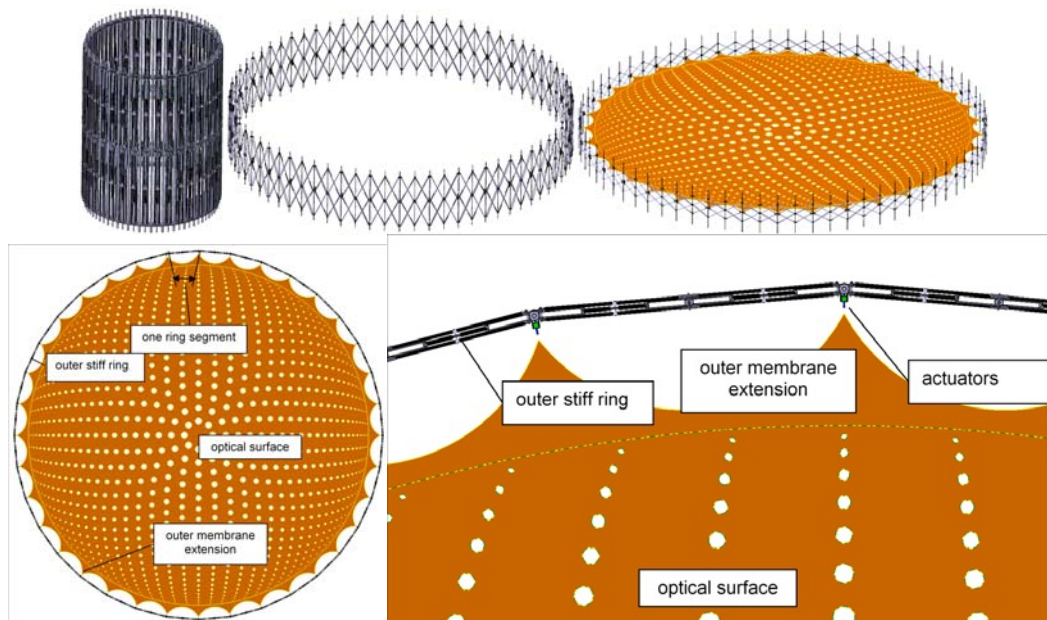

Fig.3. Deployable pantograph stretching the membrane and detail on the control-actuators on the ring

C. Thermo-mechanical aspects

The diffractive lens can be approached as an homogeneous material, which will probably the case for a surface relief diffractive lens with continuous substrate. The homogenous material allows implementing a macroscopic stress field analysis and asses the possibility to deploy a wrinkle free, planar membrane.

For Fresnel zone plate type lens like photon sieve the mechanical modeling needs unaffordable numerical efforts. Indeed, in the photon sieve telescope concept the ratio between the overall size and the smallest feature size (telescope diameter 10 m over the perforation hole-diameter 10 µm) is in the order of 10^6. In addition, taking into account the number of the holes (10^9) in the perforated surface, it makes the detailed FEM modeling and analysis of the telescope impossible (with the available computational power and time). Therefore a multi level structural FEM analysis with the following steps has been carried out to study the thermo-mechanical behavior of the telescope structure:

- Micro-mechanical FEM homogenization analyses of the reinforcement biaxially woven fabric composite, derivation of effective ABD stiffness matrix (inverse of the compliance matrix)
- Repeated unit cell analyses of the membrane laminate: with the hole pattern implemented, an aluminum layer and the fabric reinforcement, symmetric, asymmetric, again, derivation of effective ABD stiffness matrices.
- Full surface modeling and FEM analysis using homogenized material properties for global performance.
- Ring performance assessment (less critical)

For the purpose the Macro-mechanical analysis, substrate thickness, the indention radius of the membrane between the support points as well as the outer edge reinforcement have been applied as design parameter. For a given value of pre-tensioning, the required tensioning forces at the support points of the pantograph ring have been determined. Furthermore, the required stroke of the tensioning actuators for compensating of static displacements as well as thermal expansion has been assessed. Instead of the pantograph ring, an equivalent dummy support has been included in the model at the 36 connection points to the pantograph ring. At these points also the pre-tensioning forces are applied.

For simplification and making the simulation efficient, the typical homogenization approach is applied. One repeated unit cell of the photon sieve is selected, and then six load cases (two in-plane tension-shear, two bending and twisting) are performed to get the material properties of the photon sieve. Another load case was applied to determine effective thermal expansion coefficients (Fig.4, Fig.5).

This allows deriving the local properties of the "meta" homogeneous materiel. For more detailed and in depth investigation of the hollow multi-layered membrane, a sector analysis has been performed. Expectedly, the perforation of the membrane leads to a non homogeneous stress field (Fig.6).
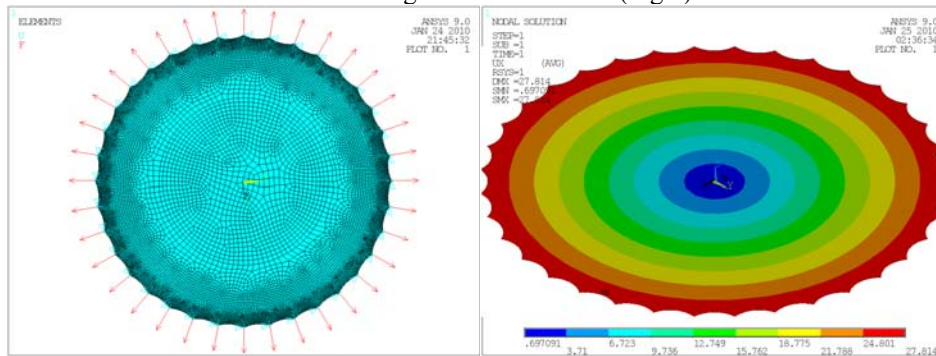

Fig.4. Thermal expansion FEM analysis of the diffractive lens membrane for a 100 K thermal load. The effect of the thermal expansion is equivalent to a change of the focal length of the lens
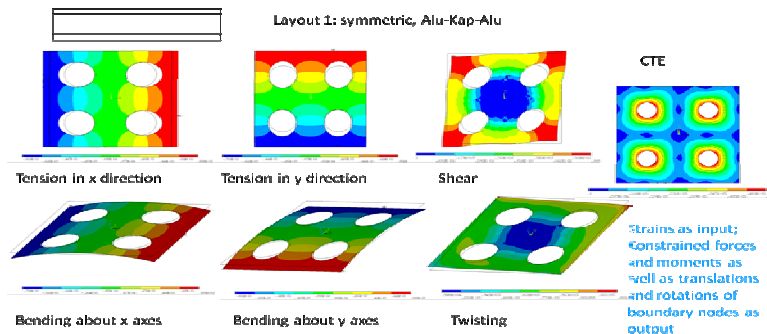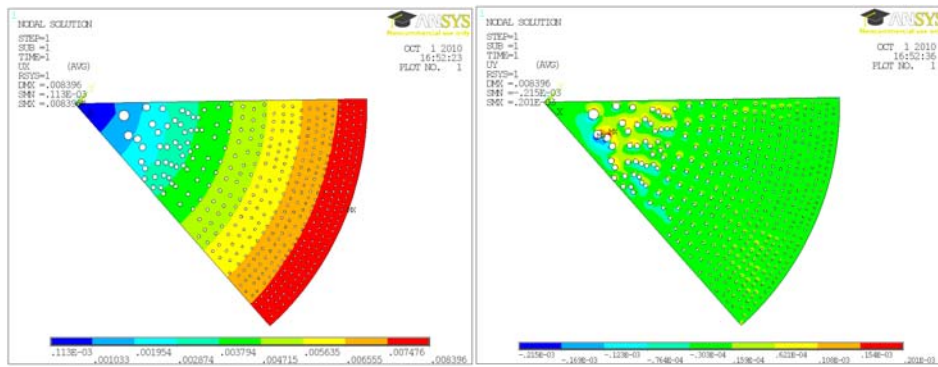

Fig.5. Example of a micro-scale analysis of the photon-sieve which is extrapolated as mechanical behaviour of an homogenous material.

Fig.6. (Left) Radial and (Right) tangential stress fields in a sector of a perforated membrane for a pre-tensioning load of 1MPa.

It is observed from Fig.6 that the resulting radial stress increases radially. Circumferential stress shows more uniform nature except some local stress variations at the larger in-homogonous hole's placement at the inner area of the sieve. Generally it looks like a homothetic scaling of the membrane, which again is optically interpreted as a change in focal length.
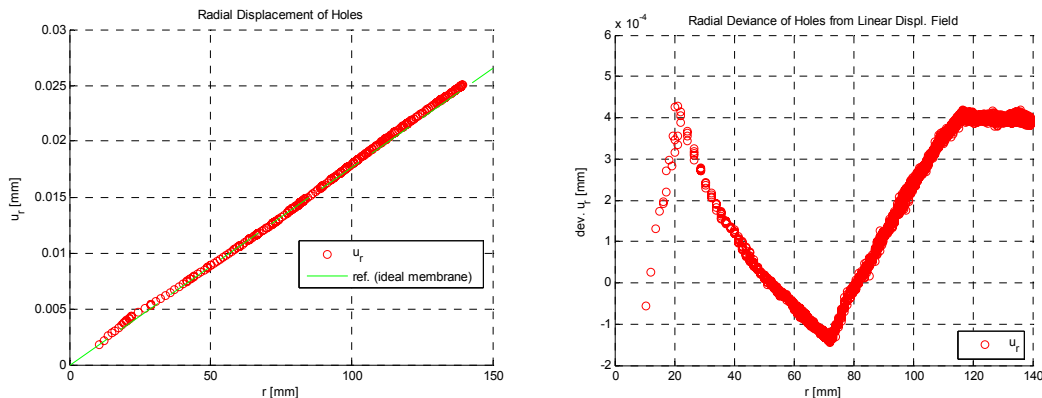
Things are not obvious anymore in the presence of inhomogeneous perforation densities in so-called anti-hole photon-sieves [13].
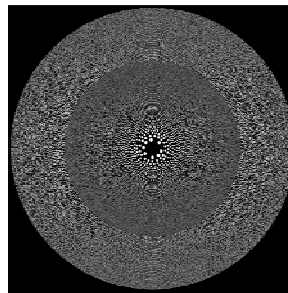
Fig.7. Photonsieve with anti-holes on the outer ring, D=0.316 m, f=31.6 m.
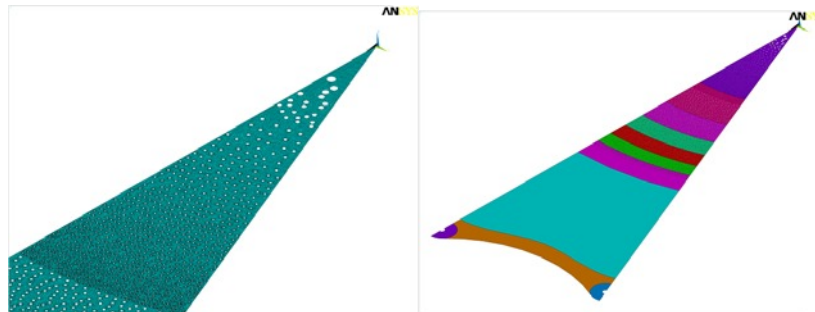
Fig.8. Section model of the anti-hole photon-sieve.

Fig.9. (Left) Radial displacement and (Right) departure from the best fit linear displacement stress field in a sector of a perforated membrane for a pre-tensioning load of 1MPa.

Fig.9 shows the deviations from the theoretical position of the perforations for the photon sieve of Fig.7. The value exceeds quickly, 10 μm accuracy. However this linear deformation is a rescaling of the lens and thus appears as a change in focal length.

The deviation with respect to the linear fit (best focus line) can be interpreted as an aberration with radial symmetry. In the above examples the departure with respect to a 10 μm position tolerance remains acceptable. These residuals are the one which can contribute to image quality degradation.

This simplified analysis aimed to illustrate some ingredients of the diffractive lens thermo-mechanical modelling. We believe that the success and feasibility of realizing deployable; diffractive lenses will rely on their thermo-elastic and finite-elements modelling, because demonstrator will have dimensional limits and cannot be tested in realistic conditions. However this will require significantly higher computational capacity.

IV. DEMONSTRATOR

A. Manufacturing

Our demonstrator is based on a F/100 photon-sieve operating at 633 nm, with smallest holes diameter of 50 μm. This resulted in a photon-sieve partially filled with anti-holes on the outer ring (Fig.7).

The demonstrator membrane had 0.316 m diameter, 31.6 m focal length @633 nm, 889600 pinholes (smallest is 48 μm), throughput 20%, diffraction efficiency 0.6%, The first sidelobes of the point spread function (PSF) do not exceed 0.1% of the central peak (contrast 1:1000). PSF FWHM=140μm

The material selection was done in second choice by the cutting facility itself. Indeed, the hole perforation strategies (wavelength, exposure time, speed) had to be implemented in terms of the heat load during cutting. Some materials required too much power, or overheated the material locally, which resulted in high statistical spread on the hole-diameters. Coupon test were done in 6 companies in Europe. Although, we contacted more than 20 companies, only a few of them were co-operative.

We selected finally a laser cutting facility using a triple YAG laser @355 nm to perforate Aluminized Kapton®. This UV radiation interacts with the material and by photo chemical ablation removes the matter.

It is possible to cut in any thin material. The maximum working area is 600 mm X 500 mm and the smallest hole that can be cut out has 20 µm diameter (a single dot). The holes are not burned, but really cut out along their circumference. (Coupon test results on Al-Kapton® Sheldahl Ref 14645 - 3.0 mils (0.075 mm) – 100 nm Al.), Relative hole position error 2 μm,. Average hole error (scaling) : 10 μm. Hole diameter StDev: 1 μm).

The overall accuracy on the maximum working surface is less than +/- 25 µm. The cutting speed (holes/second) depends on too many parameters and cannot be given before doing some experiments on the dedicated material of our application. In order to avoid overheating of the membrane during manufacturing cutting-speed was slow. The full perforation process took 3 weeks.

Fig.10.   From top left to bottom right: (a) Photon-sieve after hole drilling, (b) details of the drilled holes, (c) un-stretched photon-sieve, (d) stretched photon-sieve, (e) mounted in support, and during optical test in front of a 300 mm optical collimator in a 40 m corridor.

B. Optical tests results

The photon-sieve end to end performances were measured in terms of point spread function and wavefront error. ACCD camera set in the best focus position and recorded the PSF. We notice here already a typical problem when working with long distances, air turbulence and convection are not negligible anymore. Precaution where taken (door closed, no human presence, in the evening when all temperature are homogenized in the room), to record a repeatable PSF signal (Fig.11). A profile of the PSF is given in Fig.12.

The second measurement was a wavefront error measurement with Shack Hartmann sensor. The measurement was done converging beam, the defocus (curvature) term is subtracted from the measurement.
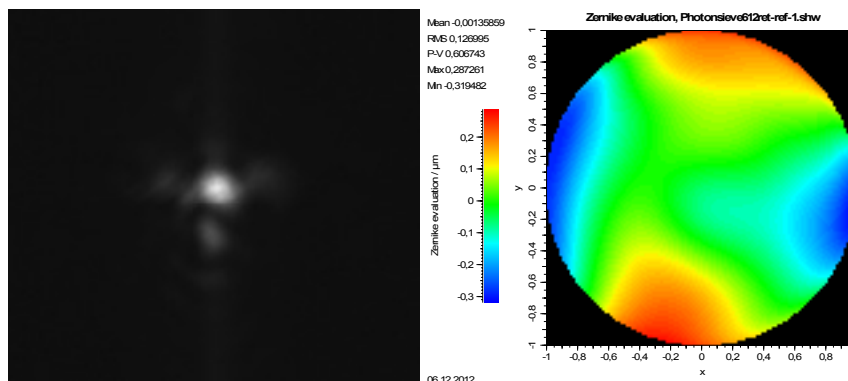

Fig.11.   (Left) Photo-sieve point spread function showing important side-lobes taken @633 nm, (Right). Wavefront error map (@633 nm) RMS=130 nm.

The PSF shows important side lobes ¨(20% of peak irradiance)) while the random distribution of the holes, and simulation confirmed this, indicate that we would have side-lobes of less than 0.1%$ of the peak irradiance.

The presence of these side-lobes can be qualitatively explained with the WFE measurement which shows that our photon-sieve is not strictly diffraction limited. The WFE is directly related to position errors of the holes. This is apparently not due to the pre-stress/tensioning mechanism. Consequently we believe that this positioning error happens during the manufacturing process, very likely because there are local thermo-elastic deformations of the membrane at that moment.
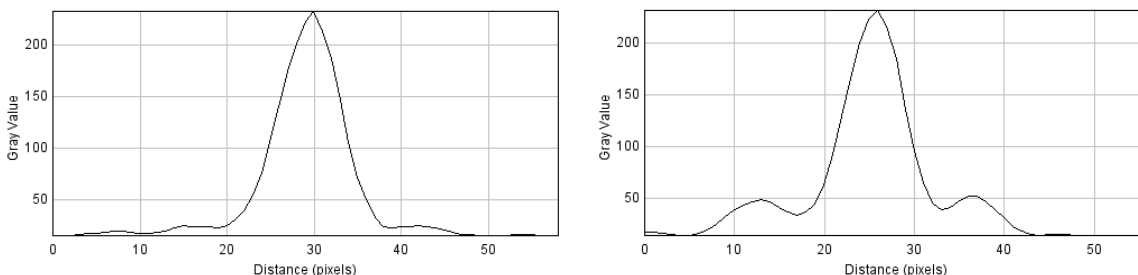

Fig.12.   (Left) Photon-sieve X-cut point spread function @633 nm, (Right) Photo-sieve Y-cut point spread function @633 nm showing important side-lobes taken @633 nm. The PSF FWHM=10 pixels=> 140 μm (Theoretical 150 μm expected). Diffraction efficiency: 0.4% < 0.6% (in theory), Contrast sidelobes: 20% (expected 0.1%).

V. CONCLUSION

This article has explored some challenge that will be faced if one plans to use large (> 10 m) deployable diffractive lens in space telescopes. It was run independently but nearly simultaneously to a study [15] in the United States on a 0.8 m phase diffractive element in polyimide, where similar challenges have been phase.

All these lenses are not necessarily cheap alternatives with respect to membrane telescopes or foldable petals. If one plans optical telescope applications one has to remind that these lenses have also:

- in-plane accuracies of the microns even for very large F-numbers (>F/20)
- out-of plane (surface relief accuracies) which are sub-micrometric, if aims high diffraction efficiency.
- a chromatic behavior, and that correction of this chromatism, makes the auxiliary optics complex
- large focal lengths (>100 m) , which will require formation flying

Although we know how to manufacture them at small scale (<1 m), they have currently not identified facilities in Europe that allow to write/perforate diffractive pattern with a micrometric accuracy on at 10 m scale. Similar limitations have been observed in the United States, where a adequate plotter manages to print a pattern to a 0.8 m scale with required in plane accuracies.

In the course of this study, we have touched a critical end to end optical testing problem, which does not appear on small-scale models (0.1m). Flight model photon sieves will very likely have diameters of at least 10 m diameter and F/20 and more, this will give a focal distances of hundred of meters , even kilometres need to be envisaged. Today there is no testing facility, which allows measuring the end to end optical performance in representative environmental conditions (space flight, thermal vacuum), with a visible collimated beam of 10 m diameter or more, and with a detector placed at 100 m. Furthermore, we are also far from representative optical measurement conditions: turbulent air flow, gravity effect on the photonsieve, thermal loads, wind, etc…

Moderate scale models (1 meter scale) and optical simulation can only asses the link between mechanical tolerances and optical performances. The validation of the in-flight end to end performances can only rely on thermo-elastic FEM models and simulations, using large computational capacity. We have no alternative today.

VI.   REFERENCES

[1].R.Hyde, Eyeglass. 1. Very Large Aperture Diffractive Telescopes, Applied Optics, Vol. 38, Issue 19, pp. 4198 (1999).
[2].United Applied Technologies, "Fresnel concentrators for Space Solar Power and Thermal Solar Propulsion", Final report (2001)
[3].G.Andersen, Large optical photon sieve, Optics Letters, Vol. 30, Issue 22, pp. 2976-2978 (2005).
[4].L.Koechlin et al., "High resolution imaging with Fresnel interferometric arrays: suitability for exoplanet detection", Astronomy and astrophysics 443, 709 (2005).
[5].D.Serre et al., "Fresnel interferometric arrays for space-based imaging: testbed results", Proc. SPIE. 6687 (2007).
[6].L.Koechlin, "The Fresnel interferometric imager", Cosmic Vision proposal, (2007).
[7].E.Hinglais et al., "Fresnel formation Flying: high resolution imager for optical astrophysics", ESA SP-654 (2008).
[8].D.Serre et al., "Fresnel interferometric imager: ground-based prototype", Appl. Opt. 48, 2811 (2009).
[9].H.Arsenault, "Diffraction theory of Fresnel Zone Plates", J. Opt. Soc. Am. 58, 1536 (1968).
[10].   D.Faklis and M. Morris, "Broadband imaging with holographic lenses", Opt. Eng. 28, 592 (1989).
[11].   A.B.Meinel, M.P.Meinel, Large membrane space optics: Imagery and aberrations of diffractive and holographic achromatized elements of high diffraction order, Opt Eng 41(8), 1995 (2002)
[12].   A.B.Meinel, M.P.Meinel, Parametric dependencies of high-diffraction-order achromatized aplanatic configuration that employ circular or cross-linear diffractive optical elements; AO 41(34), 7155 (2002).
[13].   G.Andersen, Broadband antihole photon sieve telescope, Applied Optics, Vol. 46, Issue 18, pp. 3706-3708 (2007).
[14].   G.Andersen, Membrane photon sieve telescopes, Applied Optics, Vol. 49, Issue 33, pp. 6391-6394 (2010).
[15].   P.Atcheson et al., MOIRE: Initial demonstrator of a transmissive diffractive membrane optic for large lightweight optical telescope, Proc. SPIE 8442, Space Telescopes and Instrumentation 2012: Optical, Infrared, and Millimeter Wave, 844221 (2012).
[16].   L.Datashvili, "Review and Evaluation of the Existing Designs and Technologies for Space Large Deployable Apertures", International Scientific Conference on Advanced Lightweight Structures and Reflector Antennas, 14-16 October, Tbilisi, Georgia, 2009
[17].   Poe, Garrett D.; Patrick, Brian G., "Zero CTE polyimides for athermal optical membranes", Novel Optical Systems Design and Optimization XI. Edited by Koshel, R. John; Gregory, G. Groot; Moore, James D., Jr.; Krevor, David H. Proceedings of the SPIE, Volume 7061, article id. 706114, 9 pp. (2008)

VII.   ACKNOWLEDGEMENTS